JACS
JOURNAL OF THE AMERICAN CHEMICAL SOCIETY
pubs.acs.org/JACS
Article

X-ray and Optical Circular Dichroism as Local and Global Ultrafast Chiral Probes of [12]Helicene Racemization

Victor M. Freixas, Jérémy R. Rouxel,* Yeonsig Nam, Sergei Tretiak,* Niranjan Govind,* and Shaul Mukamel

Cite This: https://doi.org/10.1021/jacs.3c07032
Read Online
ACCESS | Metrics & More | Article Recommendations | Supporting Information

ABSTRACT: Chirality is a fundamental molecular property that plays a crucial role in biophysics and drug design. Optical circular dichroism (OCD) is a well-established chiral spectroscopic probe in the UV−visible regime. Chirality is most commonly associated with a localized chiral center. However, some compounds such as helicenes (Figure 1) are chiral due to their screwlike global structure. In these highly conjugated systems, some electric and magnetic allowed transitions are distributed across the entire molecule, and OCD thus probes the global molecular chirality. Recent advances in X-ray sources, in particular the control of their polarization and spatial profiles, have enabled X-ray circular dichroism (XCD), which, in contrast to OCD, can exploit the localized and element-specific nature of X-ray electronic transitions. XCD therefore is more sensitive to local structures, and the chirality probed with it can be referred to as local. During the racemization of helicene, between opposite helical structures, the screw handedness can flip locally, making the molecule globally achiral while retaining a local handedness. Here, we use the racemization mechanism of [12]helicene as a model to demonstrate the capabilities of OCD and XCD as time-dependent probes for global and local chiralities, respectively. Our simulations demonstrate that XCD provides an excellent spectroscopic probe for the time-dependent local chirality of molecules.

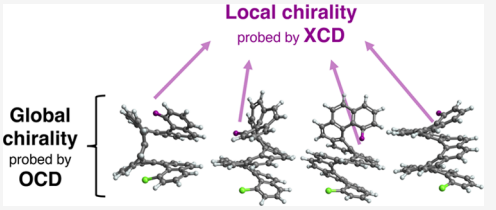

I. INTRODUCTION

Chirality is a geometrical property of objects that does not coincide with their mirror image, which is essential to chemical and biological functions of molecules.[1] Most enzymes, amino acids, carbohydrates, nucleosides, and some hormones are chiral.[2] The origin of the homochirality of life, that living organisms only contain L-amino acids and D-sugars,[3] remains a mystery.[4,5] More than half the modern drugs are chiral,[6] and chirality control is therefore crucial for drug design. In most cases, drugs are used therapeutically as racemates, but there are cases where only one enantiomer is medically active, while the other is inert or even harmful.[7] Probing molecular chirality is of vital importance, and the United States Food and Drug Administration (US FDA) requires early establishment of the absolute stereochemistry for all chiral drugs.[8]

In contrast to ensembles of achiral molecules, chiral molecules interact differently with other chiral objects, such as circularly polarized light, which depends on the sense of polarization. The circular dichroism signal (CD) is defined as the difference between the absorption of left- and right-handed circularly polarized light and is widely used for the infrared to near-ultraviolet (UV) detection of molecular chirality.[9,10] CD is then denoted optical circular dichroism (OCD). While chirality commonly relies on a chiral center, global chiral geometries such as axial, planar, propeller-type, and helical are known as well.[11] Helicenes (Figure 1) are important examples of molecules with helical chiral geometry.[12−16] These are highly conjugated systems, where the electronic and magnetic allowed transitions are distributed over the entire molecule, and the OCD signal thus probes its global chirality.

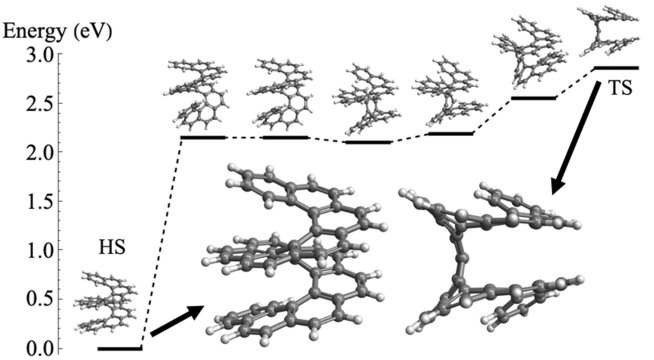

Figure 1. Racemization pathway of [12]helicene. The data for molecular structures and respective energies are taken from the work of Barroso and co-workers.[39]

Received: July 3, 2023

Recent advances in polarization control and the spatial profile of X-ray beams enable the study of molecular chirality in the X-ray regime.[17,18] The probes then can be tuned to be resonant with core electronic transitions,[19] which are element-selective and are therefore highly local in nature.[20] In particular, if the molecule has a single chromophore with a distinct core transition, the corresponding excitations can be related to chromophore localization in real space. X-ray circular dichroism (XCD) should therefore be more sensitive to the local molecular structure.[21] In this work, we show that OCD and XCD are complementary, enabling the time-dependent study of both global and local chiral features.

Helicene chemistry is a rapidly growing field[22−31] with applications to asymmetric catalysis,[32] nonlinear optics,[33] spin filters,[34] switches and sensors,[35] and the design of molecular machines.[12] They can be synthesized with different sizes and are usually referred to as [n]helicenes, where n denotes the number of benzene rings. Due to their unique geometric features, helicenes have been widely studied for several decades. The partial racemization of [6]helicenes between the two helical enantiomers was detected in 1956 while determining its melting point.[36] Few years later, the kinetics of the thermal racemization of a series of [n]helicenes (with n = 6−9) was studied.[37,38] The most likely hypothesis underpinning the inversion dynamics is a specific conformational pathway.[39] For [5]helicene, a mechanism involving a planar C_{2v} transition state (TS) was proposed; however, for [n]helicene (with $n \geq 6$), steric hindrance forbids a planar TS. A nonchiral C_s TS was found for [6]helicene.[40] In 1996, the barriers along the inversion paths were computed for n = 3−6 and 8 and showed a steady increase up to n = 6 and a plateau for $n > 6$.[41] The barriers for [9]helicene were computed in the same year, indicating another local minimum in the vicinity of TS.[42] In 2018, the inversion mechanism was revisited and generalized for arbitrarily large n, involving $2n - 14$ intermediate states for $n \geq 8$.[39]

In this paper, we use [12]helicene to explore the capabilities of OCD and XCD as ultrafast probes for the global and local chiralities along its chiral transition from TS (right magnified sketch in Figure 1) to the single helix-shaped (HS) configuration (left magnified sketch in Figure 1). The half inversion pathway, calculated by Barroso and co-workers,[39] includes several intermediates, as depicted in Figure 1, and shows a set of alternating local barriers and minimum energy structures. The TS appears in the middle of the racemization pathway and lies at the highest conformational energy barrier with C_s symmetry. Although this global structure is achiral, from the local point of view, it can be understood as a joint pair of symmetric helicenes with opposite twists, hence having an opposite local chirality. In contrast to TS, the HS conformer of [12]helicene has the same chirality from both global and local points of view, since the twist is in the same direction across the entire molecular structure. Given its unique geometrical properties and racemization mechanism, this molecule is ideally suited for exploring the interplay between the time-dependent global and local chiralities by using the OCD and XCD techniques, respectively.

Although core excitations of chemically equivalent carbon atoms can be resolved in some systems (for example, in the ESCA molecule),[43−46] the small chemical shift between all C atoms in helicene does not allow for resolving them separately and use them as local windows in XCD. To use the XCD capabilities as a local probe, we substitute some H atoms by either F or Cl or both that serve as X-ray chromophores at different positions along the molecule. We label these substitution sites along the molecular structure, as shown in the inset of Figure 2a, by H atom coloring. For substituted

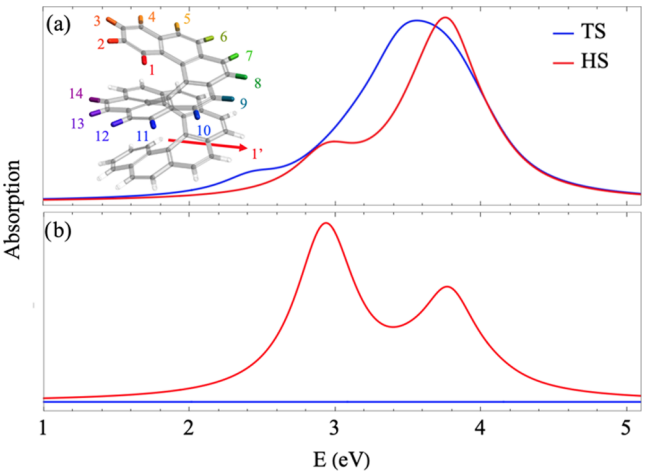

Figure 2. Calculated (a) absorption and (b) circular dichroism (OCD) spectra for the TS and HS conformers of [12]helicene. The inset in (a) shows the site coloring label for F and Cl chromophore substitutions (see Figures 3 and S1).

systems with a single X-ray chromophore (F or Cl), the corresponding XCD signals can be obtained at either F or Cl K-edges and thus are unequivocally related to the local chirality near the selected chromophore.

We have analyzed XCD as a function of the substitution site for each chromophore (F and Cl). To explore how the [12]helicene racemization takes place, we have simulated its thermal relaxation from the TS to HS conformation when a F atom is substituted on site 1 and a Cl atom is substituted on site 1′, forming symmetric counterparts. The corresponding OCD and XCD signals for the structures along this molecular dynamics trajectory illustrate their roles as global and local time-dependent chirality probes. This is the main result of this work. The rest of the article is organized as follows: In Section II, we present the expressions required for calculating the OCD and XCD signals. In Section III, we summarize our results and conclude in Section IV. Computational details are given in Section V.

II. OCD AND XCD SIGNALS

The circular dichroism (CD) signal is defined as the difference in the absorption spectra of left and right circularly polarized probe pulses. The interaction between the molecule and light is given by the following Hamiltonian

$$H = H_0 - \boldsymbol{\mu}\cdot\boldsymbol{E} - \boldsymbol{m}\cdot\boldsymbol{B} \quad (1)$$

where H_0 represents an isolated molecule, $\boldsymbol{E}$ and $\boldsymbol{B}$ are, respectively, the electric and magnetic fields of the incoming pulse, and $\boldsymbol{\mu}$ and $\boldsymbol{m}$ are the corresponding transition dipoles. We neglect the electric quadrupole moment, since its contribution to the CD signal vanishes in isotropic randomly oriented ensembles.[47] The absorption of a weak left (L) circularly polarized probe with frequency ω is given by

$$A^{\mathrm{L}}(\omega) = 2\omega\mathrm{Im}\{\boldsymbol{E}^{\mathrm{L}^*}(\omega)\cdot\boldsymbol{P}^{\mathrm{L}}(\omega) + \boldsymbol{B}^{\mathrm{L}^*}(\omega)\cdot\boldsymbol{M}^{\mathrm{L}}(\omega)\} \quad (2)$$

https://doi.org/10.1021/jacs.3c07032
J. Am. Chem. Soc. XXXX, XXX, XXX−XXX

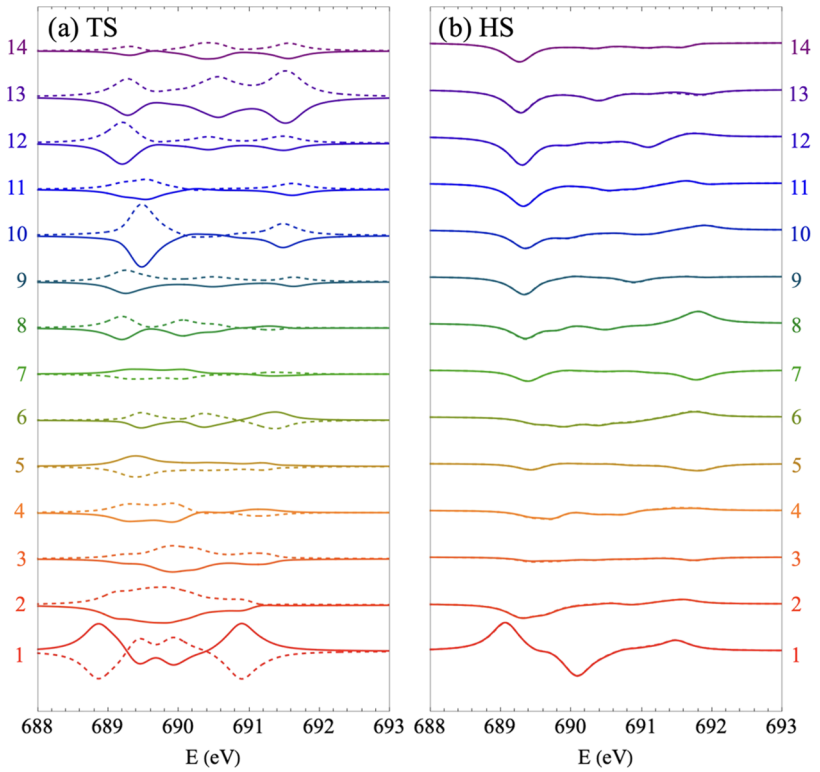

Figure 3. Solid lines: calculated XCD spectra for the (a) TS and (b) HS structures substituted with a F atom at different positions (as labeled in the inset of Figure 2b). Dashed lines: same for substitutions at the symmetric counterpart positions.

where Im stands for the imaginary part and $\boldsymbol{P}^{\mathrm{L}}$ and $\boldsymbol{M}^{\mathrm{L}}$ are the electronic polarization and magnetization induced by the left circularly polarized probe, respectively. The right (R) circularly polarized absorption spectrum is given by the same expression by substituting the L index with R. The CD signal S_{CD} is finally given by[9]

$$S_{\mathrm{CD}}(\omega) = 2\omega\mathrm{Im}\{\boldsymbol{E}^{\mathrm{L}^*}(\omega)\cdot\boldsymbol{P}^{\mathrm{L}}(\omega) - \boldsymbol{E}^{\mathrm{R}^*}(\omega)\cdot\boldsymbol{P}^{\mathrm{R}}(\omega) + \boldsymbol{B}^{\mathrm{L}^*}(\omega)\cdot\boldsymbol{M}^{\mathrm{L}}(\omega) - \boldsymbol{B}^{\mathrm{R}^*}(\omega)\cdot\boldsymbol{M}^{\mathrm{R}}(\omega)\} \quad (3)$$

By expanding the polarization and magnetization to the first order in the incoming fields, the rotationally averaged CD signal reduces to

$$S_{\mathrm{CD}}(\omega) \propto \sum_m R_{m0}\sigma_{m0}(\omega) \quad (4)$$

where R_{m0} is the rotatory strength of the transition from the ground state to the electronically excited state m[9,48]

$$R_{m0} = \mathrm{Im}\{\boldsymbol{\mu}_{m0}\cdot\boldsymbol{m}_{m0}\} \quad (5)$$

and $\sigma_{m0}(w)$ is a Lorentzian line shape centered at the corresponding transition frequency w_{m0}

$$\sigma_{m0}(w) = \frac{\Gamma_{m0}}{(w - w_{m0})^2 + \Gamma_{m0}^2} \quad (6)$$

where Γ_{m0} is the dephasing rate. This expression holds for both OCD and XCD, with the respective frequency probing the relevant electronic transitions. The parameters used in this study can be found in the Methods section.

The sensitivity of a CD experiment can be quantified by the anisotropy factor g,[49] defined as

$$g = \frac{2(A^{\mathrm{L}} - A^{\mathrm{R}})}{A^{\mathrm{L}} + A^{\mathrm{R}}} = \frac{\boldsymbol{\mu}\cdot\boldsymbol{m}}{\boldsymbol{\mu}^2} \quad (7)$$

Good agreement between simulations and experiments has been reported in the study of OCD of ligand−protein interactions and secondary and tertiary structures of proteins[50] and in the ultrafast molecular structural changes observed by time-resolved vibrational OCD.[51] There are, however, comparatively fewer simulations reported in the X-ray region, since intense circularly polarized X-ray beams have only become available recently.[52] Furthermore, the relationship among the XCD signals, molecular geometry, and electronic structure is yet to be established.[21]

III. RESULTS AND DISCUSSION

Calculated UV absorption spectra and the corresponding OCD signals for the TS and HS conformers are shown in Figure 2. The absorption spectra shown in Figure 2a have two peaks for both conformers, which are slightly broadened and red-shifted for the TS conformation. The two OCD peaks in the OCD spectrum shown in Figure 2b are in good agreement with previous calculations for the HS structure.[53] Figure 2b also shows that only HS is a global chiral structure, while TS has a vanishingly small OCD, as expected from its C_s symmetry. For the HS conformation, the anisotropy factor has a maximum value of ∼5.1%, in good agreement with previous calculations for [10]helicene.[49]

To illustrate the capacity of the XCD as a local chirality probe, Figure 3 shows the XCD signals calculated by substituting a H atom with a F atom at different positions along the TS and HS structures. The site substitution labeling is given in the inset of Figure 2a. XCD signals for substitutions in the labeled sites and their symmetric counterparts are shown

https://doi.org/10.1021/jacs.3c07032
J. Am. Chem. Soc. XXXX, XXX, XXX−XXX

by solid and dashed lines, respectively. As previously reported, there is a strong dependence of the XCD on the substituted site.[21] The antisymmetry of all XCD signals for symmetric substitutions in TS (Figure 3a) indicates that XCD can successfully probe the local chirality of TS, which is the opposite for the top and bottom halves of the structure. Furthermore, the signals for single substitutions at symmetric counterpart sites of the HS conformation overlap almost perfectly (Figure 3b), indicating that the XCD signals probe the same local chirality at opposite parts of the HS conformation, as expected from it having the same handedness along the complete molecular structure. While there are some differences in the peak positions and intensities of the two structures, the same general trends can be seen in the solid lines, which correspond to substitutions at various sites of the molecular structure with the same sense of twist. In particular, the XCD signal for the system with the F atom substituted at position 1 is relatively strong, and the ∼689 eV peak remains approximately at the same position and intensity. The anisotropy factor in this case had a maximum of ∼0.2% for all transitions studied.

In Figure S1 in the Supporting Information, we show the calculated XCD signals when a Cl atom is substituted at different positions of the TS and HS structures. Similar to the F substitutions, the antisymmetry and symmetry for the TS and HS XCD signals reveal that the Cl atom may also be used as a sensitive probe of the local chirality of the system. In this case, Cl substitutions lead to different structures of the peaks present in the XCD spectra compared to their F-substituted counterparts. The anisotropy factor in this case has a maximum of ∼1.3% for all studied transitions.

To further investigate the capabilities of XCD to describe the local chirality of the system, we considered double substitutions at TS on site 1 and its symmetric counterpart 1′ (see the inset of Figure 2). When the same chromophore is used for the double substitutions, the electronic transitions from the corresponding cores become degenerate with opposite rotatory strengths, which vanish the XCD signal. This is formally equivalent to stating that the local chiralities, symmetrical with respect to both sides of the TS structure, cancel out when using the same probing chromophore. Double substitutions with different chromophores are required to avoid this cancellation.

We now turn to the doubly substituted system having a F atom on site 1 and Cl on its symmetric counterpart site 1′ (see the insets of Figures 2a and 4). We carried out ground-state molecular dynamics simulations with a Langevin thermostat at 300 K starting from TS. Although the F and Cl substitutions slightly change the energy landscape, the racemization pathway is expected to be similar. Since TS is located at the top of an energy barrier, thermal fluctuations drive the system away from this point to either side and through the alternated set of smaller barriers and local minima until it finally reaches the HS conformation. These simulations thus mimic the second stage of the racemization process,[39] while the first is expected to be similar but backward. Figure 4 shows the time evolution of the ground-state potential energy fluctuations with respect to the initial TS energy.

Typical snapshots along the racemization pathway are displayed in the insets of Figure 4. We see that the mean value of the energy fluctuations decreases slowly until ∼165 ps, whereas a sudden drop reflects the final transition to HS. The twist inversion occurs on the F side. The time evolution of the

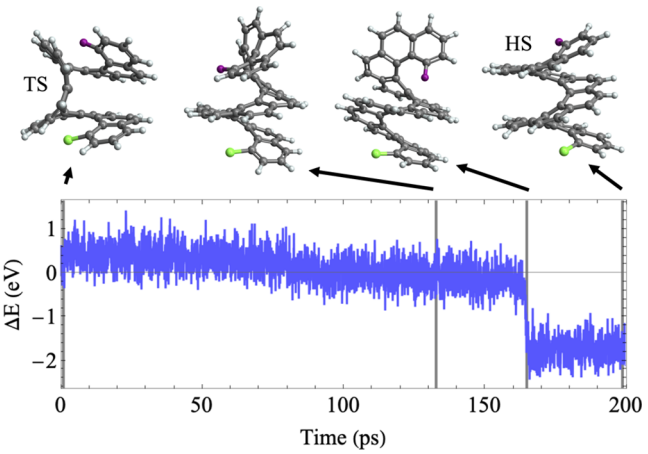

Figure 4. Time evolution of the potential energy fluctuations for ground-state molecular dynamics with a Langevin thermostat at 300 K. The initial structure is a double-substituted TS with Cl (green) and F (purple) atoms at the farthest opposite positions (site 1 and its symmetric counterpart 1′, respectively). The top structures show selected snapshots along the dynamics, at times denoted by the vertical lines.

potential energy is in good agreement with the racemization pathway previously proposed[39] and depicted in Figure 1, whereby the system has to go through several lower barriers and local minima until its final transition to the HS structure, which is found to be ∼2.5 eV down from TS, while the final transition step is calculated downhill by ∼2.2 eV.[39]

The time-dependent signals of the OCD and XCD signals along the molecular dynamics simulation depicted in Figure 4 illustrate their roles as global and local time-resolved probes, as shown in Figure 5. Figure S2 in the Supporting Information depicts some cuts corresponding to the snapshots shown in Figure 4. Figure 5a shows the time-resolved OCD signal, which starts from a blurry landscape of contributions with peaks with alternating signs induced by thermal fluctuations. As the

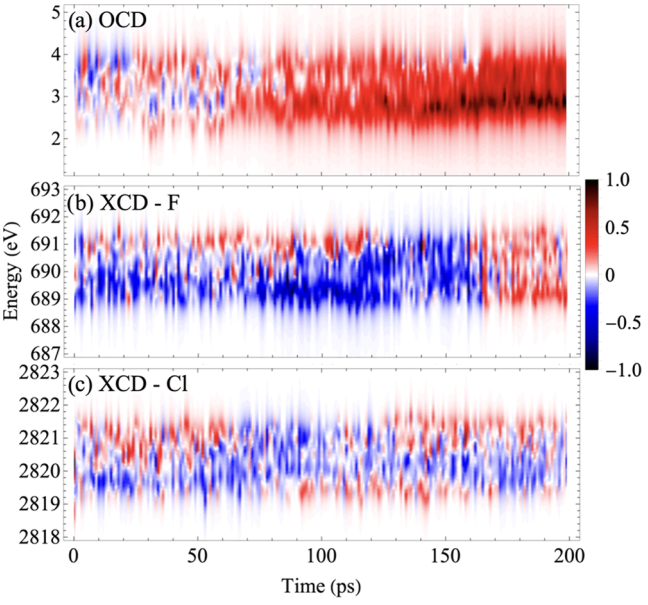

Figure 5. Time evolution of the (a) OCD signal, (b) the F K-edge XCD signal, and (c) the Cl K-edge XCD signal. The color bar indicates the normalized intensity of the signals.

https://doi.org/10.1021/jacs.3c07032
J. Am. Chem. Soc. XXXX, XXX, XXX−XXX

system goes from the globally achiral TS to HS, the chiral HS conformation peak (Figure 2b) emerges and slowly grows above thermal fluctuations until it becomes well resolved after ∼80 ps. This demonstrates the ability of the OCD signal to probe the smooth increase of the length of one side of [12]helicene with a given handedness while diminishing the other side with the opposite handedness. This, however, also implies that the OCD signal is not able to pinpoint the final transition step to the HS conformation marked by the sudden potential energy drop in Figure 4.

Figure 5b displays the time evolution of the XCD near the F K-edge, which geometrically is on the side of the local twist transition. Despite several thermal fluctuations, the ∼689 eV peak (Figure 3) has a pronounced contribution from the beginning of the trajectory, and its sign remains the same until ∼165 ps, where a sudden inversion takes place concomitant with a sudden drop of the potential energy (see Figure 4), corresponding to the final transition to the HS conformation. This demonstrates that the XCD signal is able to characterize the local chirality even through a chiral transition in the presence of thermal fluctuations.

Finally, Figure 5c shows the time-resolved XCD signal in the Cl K-edge regime. Despite several peak alternations along the dynamics, the main feature remains intact, and its sign has no significant change at ∼165 ps, indicating that the final transitions to HS taking place on the other side of the molecule only have a minor impact on the XCD signal tailored by the specific position of the Cl atom.

IV. CONCLUSIONS

Probing molecular chirality is an important fundamental task with many practical applications. Both, time-resolved OCD and XCD spectra are sensitive markers of dynamic conformational structures. OCD probes interrogate delocalized transitions that cannot carry information about the local chiral structures within a molecule. The recent development of X-ray free-electron laser (XFEL) sources has provided high light probes of XCD, which are sensitive to the local chirality of molecules.

In this theoretical study, we have compared the roles of XCD and OCD as time-dependent probes for global and local chiralities in [12]helicene, which undergoes partial racemization near its melting point. We substituted F and Cl atoms at selected positions of [12]helicene, allowing the association of XCD signals with the local chirality around the substitution. We calculated the XCD signals along the second half of the racemization pathway of the [12]helicene molecule, which starts from a globally achiral TS and evolves to the chiral HS configuration. The final transition to the HS conformer occurred at ∼165 ps. OCD probes the global chirality, showing a smooth increase along the transition. The XCD spectra in the region of the F atom K-edge show a sudden change at ∼165 ps concomitant with the final transition to HS. XCD in the Cl K-edge regime shows approximately the same behavior throughout the dynamics. Our findings reveal that XCD signals are a sensitive spectroscopic technique to probe the time-dependent local chirality of molecular materials, even for a chiral transition in the presence of thermal fluctuations. In all cases, the anisotropy factor is large enough to make these experiments feasible, providing the basis for using XCD signals as local windows to probe the dynamics of chiral systems at XFEL and synchrotron facilities.

V. METHODS

Single-point calculations for the transition dipoles and rotatory strengths were performed at the time-dependent density functional theory (TDDFT) level using the B3LYP[54−57] exchange−correlation functional as implemented in the NWChem computational chemistry program.[58] We employ the 6-31G*[59−61] basis set for H and C atoms and the Sapporo-TZP-2012[62] basis set for F and Cl. All basis sets were obtained from the Basis Set Exchange.[63−66] We computed 30 excited states for the UV regime and 10 excited states for each of the X-ray regime calculations. For the calculation of transition dipoles, we used the gauge-including atomic orbital (GIAO) approach[67] in order to avoid the origin dependence of magnetic properties.[21,68−71]

The dephasing rate Γ_{m0} (see eq 6) was set to 0.5 eV. The computed X-ray spectra with NWChem[19,72] were shifted by 20 and 60 eV for the energy of the transitions in the region of the F and Cl atom K-edges, respectively. The calculated peaks of the X-ray absorption near edge structure (XANES), shown in Figure S3, without these shifts, match experimental mean values for systems having similar bonds and aromaticity.[73,74]

Ground-state molecular dynamics with the Langevin thermostat was simulated with the NEXMD software package,[75] setting the time step to 0.5 fs, the temperature to 300 K, and the Langevin friction coefficient to 20 ps^{-1} and using the semiempirical Austin Model 1 (AM1) Hamiltonian.[76] The initial structure of TS, as well as the racemization pathway and corresponding energies, is taken from the supplementary information of the work of Barroso and co-workers.[39]

■ ASSOCIATED CONTENT

Supporting Information

The Supporting Information is available free of charge at https://pubs.acs.org/doi/10.1021/jacs.3c07032.

Time evolution (MP4)

XCD spectra for [12]helicene substituted with Cl, OCD, and XCD snapshots and X-ray absorption near edge structure (XANES) (PDF)

■ AUTHOR INFORMATION

Corresponding Authors

Jérémy R. Rouxel − *Chemical Sciences and Engineering Division, Argonne National Laboratory, Lemont, Illinois 60439, United States*; Email: jeremy.rouxel@univ-st-etienne.fr

Sergei Tretiak − *Theoretical Division, Los Alamos National Laboratory, Los Alamos, New Mexico 87545, United States*; orcid.org/0000-0001-5547-3647; Email: serg@lanl.gov

Niranjan Govind − *Physical and Computational Sciences Directorate, Pacific Northwest National Laboratory, Richland, Washington 99352, United States; Department of Chemistry, University of Washington, Seattle, Washington 98195, United States*; orcid.org/0000-0003-3625-366X; Email: niri.govind@pnnl.gov

Authors

Victor M. Freixas − *Department of Chemistry and Physics and Astronomy, University of California, Irvine, California 92697-2025, United States*; orcid.org/0000-0003-1733-4827

Yeonsig Nam − *Department of Chemistry and Physics and Astronomy, University of California, Irvine, California 92697-2025, United States*; orcid.org/0000-0003-0386-9118

Shaul Mukamel − *Department of Chemistry and Physics and Astronomy, University of California, Irvine, California 92697-2025, United States*; orcid.org/0000-0002-6015-3135

https://doi.org/10.1021/jacs.3c07032
J. Am. Chem. Soc. XXXX, XXX, XXX−XXX

Complete contact information is available at: https://pubs.acs.org/10.1021/jacs.3c07032

Notes

The authors declare no competing financial interest.

■ ACKNOWLEDGMENTS

This work was primarily supported by the U.S. Department of Energy (DOE), Office of Science, Office of Basic Energy Sciences, Division of Chemical Sciences, Geosciences, and Biosciences under DE-SC0022225 (V.F., Y.N., and S.M.), DE-FG02-04ER15571 (S.M.), FWP 72684 (N.G.), and FWP LANLE3T1 (S.T.). S.M. gratefully acknowledges the support of NSF through award CHE-2246379 and the Hagler Institute for Advanced Study at Texas A&M University, where he is a fellow. This work benefited from high-performance computing resources provided by the University of California, Irvine (UCI), the Environmental Molecular Sciences Laboratory (EMSL), a DOE User Facility sponsored by the Office of Biological and Environmental Research (BER) and located at PNNL, which is operated by Battelle Memorial Institute under Contract No. DE- AC05-76RL1830, and the National Energy Research Scientific Computing Center (NERSC), a DOE User Facility operated under Contract No. DE-AC02-05CH11231. This research was also performed in part at the Center for Integrated Nanotechnologies (CINT), a U.S. Department of Energy, Office of Science User Facility at LANL.

■ REFERENCES

(1) Hicks, J. M. *Chirality: Physical Chemistry*; American Chemical Society: Washinton, DC, 2002; Vol. *810*.
(2) Nguyen, L. A.; He, H.; Pham-Huy, C. Chiral drugs: an overview. *Int. J. Biomed. Sci.: IJBS* **2006**, *2*, 85−100.
(3) Kumari Rayala, V. P.; Kandula, J. S.; Radhakrishnanand, P. Advances and challenges in the pharmacokinetics and bioanalysis of chiral drugs. *Chirality* **2022**, *34*, 1298−1310, DOI: 10.1002/chir.23495.
(4) Podlech, J. New insight into the source of biomolecular homochirality: An extraterrestrial origin for molecules of life? *Angew. Chem., Int. Ed.* **1999**, *38*, 477−478.
(5) Quack, M. How important is parity violation for molecular and biomolecular chirality? *Angew. Chem., Int. Ed.* **2002**, *41*, 4618−4630.
(6) Rentsch, K. M. The importance of stereoselective determination of drugs in the clinical laboratory. *J. Biochem. Biophys. Methods* **2002**, *54*, 1−9, DOI: 10.1016/S0165-022X(02)00124-0.
(7) Eriksson, T.; Björkman, S.; Roth, B.; Fyge, Å.; Höuglund, P. Stereospecific determination, chiral inversion in vitro and pharmacokinetics in humans of the enantiomers of thalidomide. *Chirality* **1995**, *7*, 44−52.
(8) H Brooks, W.; C Guida, W.; G Daniel, K. The significance of chirality in drug design and development. *Curr. Top. Med. Chem.* **2011**, *11*, 760−770, DOI: 10.2174/156802611795165098.
(9) Berova, N.; Nakanishi, K.; Woody, R. W. *Circular Dichroism: Principles and Applications*; John Wiley & Sons, 2000.
(10) Lázár, A.; Angyán, J. G.; Hollósi, M.; Huszthy, P.; Surján, P. R. Theoretical CD spectrum calculations of the crown-ether aralkylammonium salt complex. *Chirality: Pharmacol., Biol., Chem. Consequences Mol. Asymmetry* **2002**, *14*, 377−385.
(11) Crassous, J. Chiral transfer in coordination complexes: towards molecular materials. *Chem. Soc. Rev.* **2009**, *38*, 830−845.
(12) Shen, Y.; Chen, C.-F. Helicenes: synthesis and applications. *Chem. Rev.* **2012**, *112*, 1463−1535.
(13) Mori, K.; Murase, T.; Fujita, M. One-step synthesis of [16]helicene. *Angew. Chem., Int. Ed.* **2015**, *54*, 6847−6851.
(14) Zhao, W.-L.; Li, M.; Lu, H.-Y.; Chen, C.-F. Advances in helicene derivatives with circularly polarized luminescence. *Chem. Commun.* **2019**, *55*, 13793−13803.
(15) Yanagi, T.; Tanaka, T.; Yorimitsu, H. Asymmetric systematic synthesis, structures, and (chir) optical properties of a series of dihetero [8]helicenes. *Chem. Sci.* **2021**, *12*, 2784−2793.
(16) Full, J.; Panchal, S. P.; Götz, J.; Krause, A.-M.; Nowak-Król, A. Modular synthesis of organoboron helically chiral compounds: cutouts from extended helices. *Angew. Chem., Int. Ed.* **2021**, *60*, 4350−4357.
(17) Alagna, L.; Prosperi, T.; Turchini, S.; Goulon, J.; Rogalev, A.; Goulon-Ginet, C.; Natoli, C. R.; Peacock, R. D.; Stewart, B. X-ray natural circular dichroism. *Phys. Rev. Lett.* **1998**, *80*, 4799.
(18) Rouxel, J. R.; Mukamel, S. Molecular chirality and its monitoring by ultrafast X-ray pulses. *Chem. Rev.* **2022**, *122*, 16802−16838.
(19) Zhang, Y.; Biggs, J. D.; Healion, D.; Govind, N.; Mukamel, S. Core and valence excitations in resonant X-ray spectroscopy using restricted excitation window time-dependent density functional theory. *J. Chem. Phys.* **2012**, *137*, No. 194306.
(20) Sessoli, R.; Boulon, M.-E.; Caneschi, A.; Mannini, M.; Poggini, L.; Wilhelm, F.; Rogalev, A. Strong magneto-chiral dichroism in a paramagnetic molecular helix observed by hard X-rays. *Nat. Phys.* **2015**, *11*, 69−74.
(21) Zhang, Y.; Rouxel, J. R.; Autschbach, J.; Govind, N.; Mukamel, S. X-ray circular dichroism signals: a unique probe of local molecular chirality. *Chem. Sci.* **2017**, *8*, 5969−5978.
(22) Schuster, N. J.; Hernández Sánchez, R.; Bukharina, D.; Kotov, N. A.; Berova, N.; Ng, F.; Steigerwald, M. L.; Nuckolls, C. A helicene nanoribbon with greatly amplified chirality. *J. Am. Chem. Soc.* **2018**, *140*, 6235−6239.
(23) Schuster, N. J.; Joyce, L. A.; Paley, D. W.; Ng, F.; Steigerwald, M. L.; Nuckolls, C. The structural origins of intense circular dichroism in a waggling helicene nanoribbon. *J. Am. Chem. Soc.* **2020**, *142*, 7066−7074.
(24) Xiao, X.; Cheng, Q.; Bao, S. T.; Jin, Z.; Sun, S.; Jiang, H.; Steigerwald, M. L.; Nuckolls, C. Single-Handed Helicene Nanoribbons via Transfer of Chiral Information. *J. Am. Chem. Soc.* **2022**, *144*, 20214−20220.
(25) Míguez-Lago, S.; Mariz, I. F.; Medel, M. A.; Cuerva, J. M.; Maçôas, E.; Cruz, C. M.; Campaña, A. G. Highly contorted superhelicene hits near-infrared circularly polarized luminescence. *Chem. Sci.* **2022**, *13*, 10267−10272.
(26) Crassous, J.; Stará, I. G.; Stary, I. *Helicenes: Synthesis, Properties, and Applications*; John Wiley & Sons, 2022.
(27) Dhbaibi, K.; Grasser, M.; Douib, H.; Dorcet, V.; Cador, O.; Vanthuyne, N.; Riobé, F.; Maury, O.; Guy, S.; Bensalah-Ledoux, A.; et al. Multifunctional Helicene-Based Ytterbium Coordination Polymer Displaying Circularly Polarized Luminescence, Slow Magnetic Relaxation and Room Temperature Magneto-Chiral Dichroism. *Angew. Chem.* **2023**, *135*, No. e202215558.
(28) Li, J.-K.; Chen, X.-Y.; Zhao, W.-L.; Guo, Y.-L.; Zhang, Y.; Wang, X.-C.; Sue, A. C.-H.; Cao, X.-Y.; Li, M.; Chen, C.-F.; et al. Synthesis of Highly Luminescent Chiral Nanographene. *Angew. Chem.* **2023**, *135*, No. e202215367, DOI: 10.1002/ange.202215367.
(29) Zhang, F.; Rauch, F.; Swain, A.; Marder, T. B.; Ravat, P. Efficient Narrowband Circularly Polarized Light Emitters Based on 1, 4-B, N-embedded Rigid Donor-Acceptor Helicenes. *Angew. Chem.* **2023**, *135*, No. e202218965, DOI: 10.1002/ange.202218965.
(30) Toya, M.; Omine, T.; Ishiwari, F.; Saeki, A.; Ito, H.; Itami, K. Expanded [2, 1][n] Carbohelicenes with 15-and 17-Benzene Rings. *J. Am. Chem. Soc.* **2023**, *145*, 11553−11565.
(31) Huang, H.-C.; Hsieh, Y.-C.; Lee, P.-L.; Lin, C.-C.; Ho, Y.-S.; Shao, W.-K.; Hsieh, C.-T.; Cheng, M.-J.; Wu, Y.-T. Highly Distorted Multiple Helicenes: Syntheses, Structural Analyses, and Properties. *J. Am. Chem. Soc.* **2023**, *145*, 10304−10313.
(32) Aillard, P.; Voituriez, A.; Marinetti, A. Helicene-like chiral auxiliaries in asymmetric catalysis. *Dalton Trans.* **2014**, *43*, 15263−15278.

(33) Verbiest, T.; Elshocht, S. V.; Kauranen, M.; Hellemans, L.; Snauwaert, J.; Nuckolls, C.; Katz, T. J.; Persoons, A. Strong enhancement of nonlinear optical properties through supramolecular chirality. *Science* **1998**, *282*, 913−915.
(34) Kiran, V.; Mathew, S. P.; Cohen, S. R.; Hernández Delgado, I.; Lacour, J.; Naaman, R. Helicenes−A new class of organic spin filter. *Adv. Mater.* **2016**, *28*, 1957−1962.
(35) Zhang, L.; Song, I.; Ahn, J.; Han, M.; Linares, M.; Surin, M.; Zhang, H.-J.; Oh, J. H.; Lin, J. π-Extended perylene diimide double-heterohelicenes as ambipolar organic semiconductors for broadband circularly polarized light detection. *Nat. Commun.* **2021**, *12*, No. 142.
(36) Newman, M. S.; Lednicer, D. The synthesis and resolution of hexahelicene1. *J. Am. Chem. Soc.* **1956**, *78*, 4765−4770.
(37) Martin, R.; Marchant, M.-J. Thermal racemisation of [6],[7], [8] and [9] helicene. *Tetrahedron Lett.* **1972**, *13*, 3707−3708.
(38) Martin, R. H.; Marchant, M. J. Thermal racemisation of hepta-, octa-, and nonahelicene: Kinetic results, reaction path and experimental proofs that the racemisation of hexa-and heptahelicene does not involve an intramolecular double diels-alder reaction. *Tetrahedron* **1974**, *30*, 347−349.
(39) Barroso, J.; Cabellos, J. L.; Pan, S.; Murillo, F.; Zarate, X.; Fernandez-Herrera, M. A.; Merino, G. Revisiting the racemization mechanism of helicenes. *Chem. Commun.* **2018**, *54*, 188−191.
(40) Lindner, H. J. Atomisierungsenergien gespannter konjugierter kohlenwasserstoffe−I: Razemisierungsenergien von helicenen. *Tetrahedron* **1975**, *31*, 281−284.
(41) Grimme, S.; Peyerimhoff, S. Theoretical study of the structures and racemization barriers of [n] helicenes (n = 3−6, 8). *Chem. Phys.* **1996**, *204*, 411−417.
(42) Janke, R. H.; Haufe, G.; Würthwein, E.-U.; Borkent, J. H. Racemization Barriers of Helicenes: A Computational Study1. *J. Am. Chem. Soc.* **1996**, *118*, 6031−6035.
(43) Siegbahn, K.; Nordling, C.; Fahlman, A. ESCA - Atomic, Molecular and Solid State Structure Studies by Means of Electron Spectroscopy. In *Nova acta regiae societatis scientiarum Upsaliensis*; Almqvist og Wiksell, 1967.
(44) Travnikova, O.; Børve, K. J.; Patanen, M.; Söderström, J.; Miron, C.; Sæthre, L. J.; Mårtensson, N.; Svensson, S. The ESCA molecule−Historical remarks and new results. *J. Electron Spectrosc. Relat. Phenom.* **2012**, *185*, 191−197, DOI: 10.1016/j.elspec.2012.05.009.
(45) Nenov, A.; Segatta, F.; Bruner, A.; Mukamel, S.; Garavelli, M. X-ray linear and non-linear spectroscopy of the ESCA molecule. *J. Chem. Phys.* **2019**, *151*, No. 114110.
(46) Mejia-Rodriguez, D.; Kunitsa, A.; Apra, E.; Govind, N. Scalable molecular GW calculations: Valence and core spectra. *J. Chem. Theory Comput.* **2021**, *17*, 7504−7517.
(47) Craig, D. P.; Thirunamachandran, T. *Molecular Quantum Electrodynamics: An Introduction to Radiation-Molecule Interactions*; Courier Corporation, 1998.
(48) Autschbach, J. Computing chiroptical properties with first-principles theoretical methods: background and illustrative examples. *Chirality: Pharmacol., Biol., and Chem. Consequences Mol. Asymmetry* **2009**, *21*, E116−E152, DOI: 10.1002/chir.20789.
(49) Nakai, Y.; Mori, T.; Inoue, Y. Theoretical and experimental studies on circular dichroism of carbo [n] helicenes. *J. Phys. Chem. A* **2012**, *116*, 7372−7385.
(50) Pecul, M.; Dzwolak, W. Optical Spectroscopy and computational methods in Biology and Medicine. In *Electronic Circular Dichroism Spectroscopy in Structural Analysis of Biomolecular Systems*; Springer Science & Business Media, 2013; Vol. *14*, pp 161−178.
(51) Rhee, H.; June, Y.-G.; Lee, J.-S.; Lee, K.-K.; Ha, J.-H.; Kim, Z. H.; Jeon, S.-J.; Cho, M. Femtosecond characterization of vibrational optical activity of chiral molecules. *Nature* **2009**, *458*, 310−313.
(52) Norman, P.; Dreuw, A. Simulating X-ray spectroscopies and calculating core-excited states of molecules. *Chem. Rev.* **2018**, *118*, 7208−7248.
(53) Furche, F.; Ahlrichs, R.; Wachsmann, C.; Weber, E.; Sobanski, A.; Vögtle, F.; Grimme, S. Circular dichroism of helicenes investigated by time-dependent density functional theory. *J. Am. Chem. Soc.* **2000**, *122*, 1717−1724.
(54) Becke, A. D. Becke's three parameter hybrid method using the LYP correlation functional. *J. Chem. Phys.* **1993**, *98*, 5648−5652.
(55) Lee, C.; Yang, W.; Parr, R. G. Development of the Colle-Salvetti correlation-energy formula into a functional of the electron density. *Phys. Rev. B* **1988**, *37*, 785−789.
(56) Vosko, S. H.; Wilk, L.; Nusair, M. Accurate spin-dependent electron liquid correlation energies for local spin density calculations: a critical analysis. *Can. J. Phys.* **1980**, *58*, 1200−1211.
(57) Stephens, P. J.; Devlin, F. J.; Chabalowski, C. F.; Frisch, M. J. Ab initio calculation of vibrational absorption and circular dichroism spectra using density functional force fields. *J. Phys. Chem. A* **1994**, *98*, 11623−11627.
(58) Edoardo, A.; Bylaska, E.; Jong, W. D.; Govind, N.; Kowalski, K.; Straatsma, T. P.; Valiev, M.; van Dam, H. J.; Alexeev, Y.; Anchell, J.; et al. NWChem: Past, present, and future. *J. Chem. Phys.* **2020**, *152*, No. 184102, DOI: 10.1063/5.0004997.
(59) Ditchfield, R.; Hehre, W. J.; Pople, J. A. Self-Consistent Molecular-Orbital Methods. IX. An Extended Gaussian-Type Basis for Molecular-Orbital Studies of Organic Molecules. *J. Chem. Phys.* **1971**, *54*, 724−728.
(60) Hariharan, P. C.; Pople, J. A. The influence of polarization functions on molecular orbital hydrogenation energies. *Theor. Chim. Acta* **1973**, *28*, 213−222.
(61) Hehre, W. J.; Ditchfield, R.; Pople, J. A. Self-Consistent Molecular Orbital Methods. XII. Further Extensions of Gaussian-Type Basis Sets for Use in Molecular Orbital Studies of Organic Molecules. *J. Chem. Phys.* **1972**, *56*, 2257−2261.
(62) Noro, T.; Sekiya, M.; Koga, T. Segmented contracted basis sets for atoms H through Xe: Sapporo-(DK)-nZP sets (n = D, T, Q). *Theor. Chem. Acc.* **2012**, *131*, 1124.
(63) Basis Set Exchange 2023 https://www.basissetexchange.org/.
(64) Feller, D. The role of databases in support of computational chemistry calculations. *J. Comput. Chem.* **1996**, *17*, 1571−1586.
(65) Schuchardt, K. L.; Didier, B. T.; Elsethagen, T.; Sun, L.; Gurumoorthi, V.; Chase, J.; Li, J.; Windus, T. L. Basis Set Exchange: A Community Database for Computational Sciences. *J. Chem. Inf. Model.* **2007**, *47*, 1045−1052.
(66) Pritchard, B. P.; Altarawy, D.; Didier, B.; Gibsom, T. D.; Windus, T. L. New Basis Set Exchange: An Open, Up-to-date Resource for the Molecular Sciences Community. *J. Chem. Inf. Model.* **2019**, *59*, 4814−4820, DOI: 10.1021/acs.jcim.9b00725.
(67) Autschbach, J. Time-dependent density functional theory for calculating origin-independent optical rotation and rotatory strength tensors. *ChemPhysChem* **2011**, *12*, 3224−3235.
(68) Naaman, R.; Beratan, D. N.; Waldeck, D. *Electronic and Magnetic Properties of Chiral Molecules and Supramolecular Architectures*; Springer Science & Business Media, 2011; Vol. *298*, pp 12−15.
(69) Krykunov, M.; Autschbach, J. Calculation of optical rotation with time-periodic magnetic-field-dependent basis functions in approximate time-dependent density-functional theory. *J. Chem. Phys.* **2005**, *123*, No. 114103.
(70) Srebro, M.; Govind, N.; De Jong, W. A.; Autschbach, J. Optical rotation calculated with time-dependent density functional theory: the OR45 benchmark. *J. Phys. Chem. A* **2011**, *115*, 10930−10949.
(71) Srebro, M.; Autschbach, J. Tuned range-separated time-dependent density functional theory applied to optical rotation. *J. Chem. Theory Comput.* **2012**, *8*, 245−256.
(72) Lopata, K.; Van Kuiken, B. E.; Khalil, M.; Govind, N. Linear-response and real-time time-dependent density functional theory studies of core-level near-edge x-ray absorption. *J. Chem. Theory Comput.* **2012**, *8*, 3284−3292.
(73) Hitchcock, A. P.; Fischer, P.; Gedanken, A.; Robin, M. Antibonding. sigma.* valence MOs in the inner-shell and outer-shell spectra of the fluorobenzenes. *J. Phys. Chem. A* **1987**, *91*, 531−540.
(74) Fujimori, T.; Tanino, Y.; Takaoka, M.; Morisawa, S. Chlorination mechanism of carbon during dioxin formation using

https://doi.org/10.1021/jacs.3c07032
J. Am. Chem. Soc. XXXX, XXX, XXX−XXX

Cl-K near-edge X-ray-absorption fine structure. *Anal. Sci.* **2010**, *26*, 1119−1125.
(75) Malone, W.; Nebgen, B.; White, A.; Zhang, Y.; Song, H.; Bjorgaard, J. A.; Sifain, A. E.; Rodriguez-Hernandez, B.; Freixas, V. M.; Fernandez-Alberti, S.; et al. NEXMD software package for nonadiabatic excited state molecular dynamics simulations. *J. Chem. Theory Comput.* **2020**, *16*, 5771−5783.
(76) Dewar, M. J.; Zoebisch, E. G.; Healy, E. F.; Stewart, J. J. Development and use of quantum mechanical molecular models. 76. AM1: a new general purpose quantum mechanical molecular model. *J. Am. Chem. Soc.* **1985**, *107*, 3902−3909.

https://doi.org/10.1021/jacs.3c07032
J. Am. Chem. Soc. XXXX, XXX, XXX−XXX

Supplementary Information: X-ray and Optical circular dichroism as local and global ultrafast chiral probes of [12]helicene racemization

Victor M. Freixas,[1] Jérémy R. Rouxel,[2, a)] Yeonsig Nam,[1] Sergei Tretiak,[3, b)] Niranjan Govind,[4, c)] and Shaul Mukamel[1]

[1)] *Department of Chemistry and Physics and Astronomy, University of California, Irvine, California 92697-2025, United States*

[2)] *Chemical Sciences and Engineering Division, Argonne National Laboratory, Lemont, Illinois 60439, USA*

[3)] *Theoretical Division, Los Alamos National Laboratory, Los Alamos, New Mexico 87545, United States*

[4)] *Physical and Computational Sciences Directorate, Pacific Northwest National Laboratory, Richland, Washington 99352, United States*[d)]

[a)]Electronic mail: jeremy.rouxel@univ-st-etienne.fr

[b)]Electronic mail: serg@lanl.gov

[c)]Electronic mail: niri.govind@pnnl.gov

[d)]Department of Chemistry, University of Washington, Seattle, Washington 98195, United States

I. XCD SPECTRA FOR [12]HELICENE SUBSTITUTED WITH CL

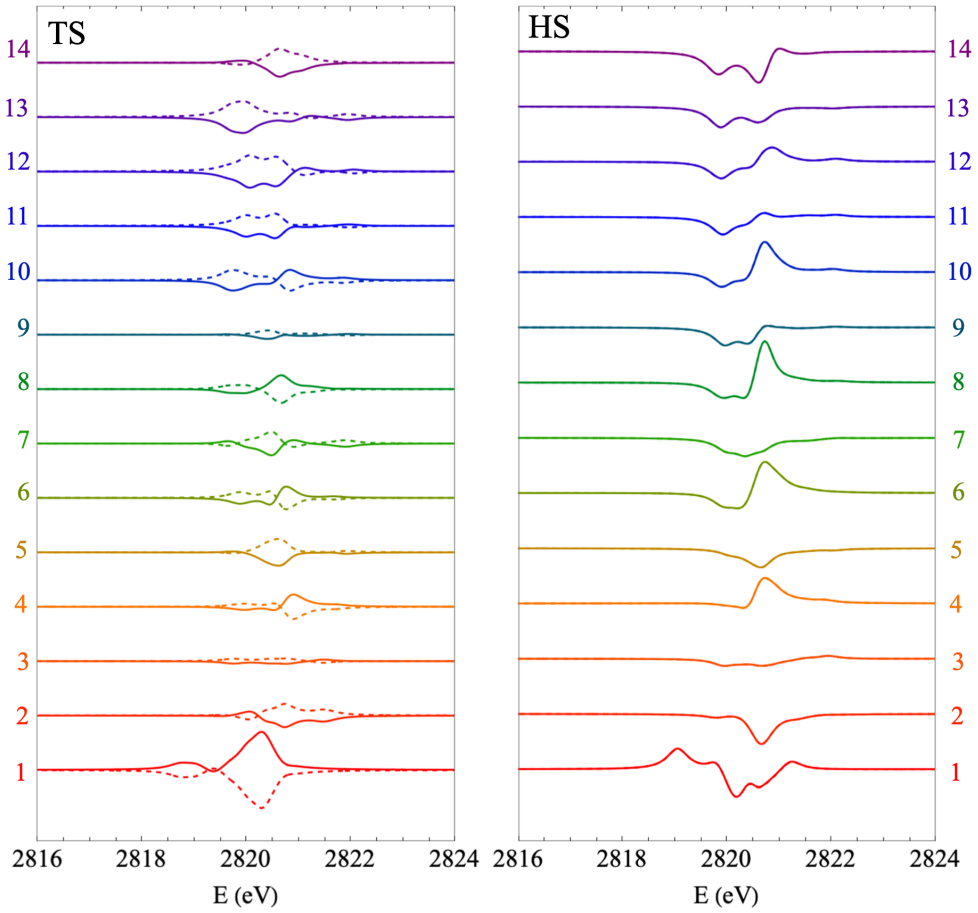

FIG. S1. Calculated XCD spectra for the TS and HS structures substituted with a Cl atom at different positions (as labeled in the inset of Figure 2 a). XCD for the symmetric substitutions are shown as dashed lines.

II. OCD AND XCD SNAPSHOTS

The different snapshots along the dynamics show the behavior of the three CD sigals. OCD (first column) grows as the system evolves from the globally achiral TS to the globally chiral HS. XCD tailored for the F K-edge transitions (second column) shows a change at the local chirality inversion, while XCD tailored for the Cl transitions (third column) remains approximately the same.

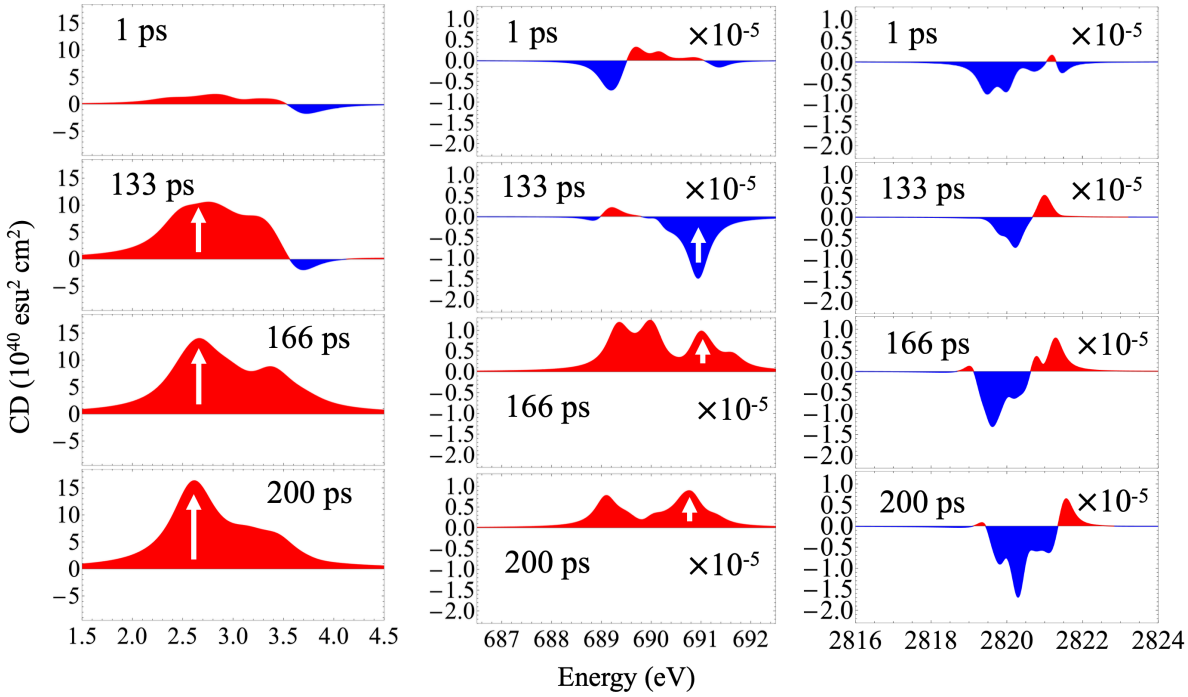

FIG. S2. Different snapshots of the time-resolved CD signals. OCD, XCD in the F-Kedge range and XCD in the Cl-Kedge range are displayed from left to right.

III. XANES

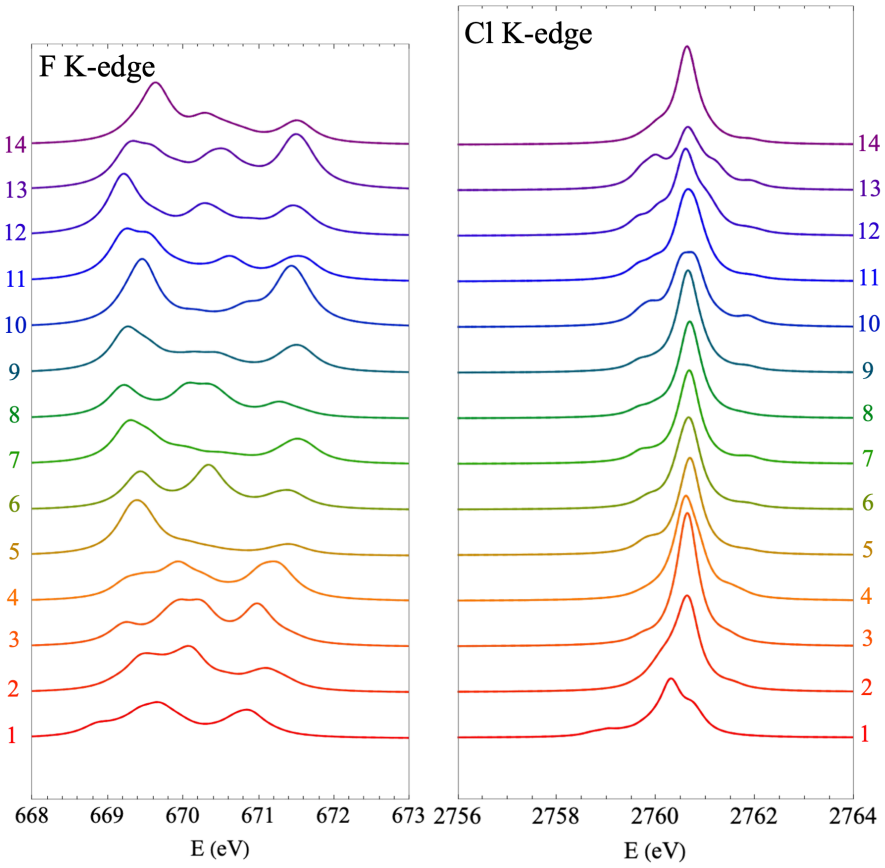

FIG. S3. XANES for the HS structure substitutions without spectral shifts.